Supplementary Information

This file contains six supplementary figures, additional references, and extended description of methods used and discussion on (1) magnetobiostratigraphy, (2) magnetic susceptibility (MS) and $CaCO_3$ weight% scales shown in Figure 1, (3) spectral results and astronomical phase relations and (4) global significance of the ETM2 event (and *Elmo* horizon).

Magnetobiostratigraphy

Discrete samples were taken from the working half cores of Site 1262 in 8 cm^3 cubes. Samples were alternating field (AF) demagnetised in steps up to 60 mT, using the "double-demagnetisation" technique[1] for AF levels above 30 mT. A drilling overprint was generally removed by 15 mT, and the remanence direction was calculated by principle component analysis[2] for steps from 20 to 40 mT (4 to 6 points). Directions with a maximum angular deviation[2] >10° were rejected. The remaining inclinations were used—along with shipboard pass-through data—to determine polarity.

The new magnetostratigraphic interpretation reveals that the *Elmo* horizon at 117.1-117.2 meters composite depth (mcd) occurs below the C24r/C24n reversal boundary at 115-116mcd (Supplementary Fig. 1) and not above as it was initially interpreted based on the shipboard measurements[3] alone. The shipboard data are noisy, presumably resulting from a combination of low magnetisation and some drilling and/or splitting related deformation. While the discrete data generally give results consistent with the shipboard results, a notable exception is Hole 1262C, on which the shipboard interpretation was largely based. In this case, the discrete samples—taken from the centre of the cores—are presumed to be less deformed than the whole core, therefore giving more reliable data. In addition, a closer examination of records indicated that the first section in Core 1262C-3H was disturbed (highlighted in Supplementary Figure 1), providing unreliable pass-through data. Taken together, discrete and pass-through data from Hole 1262B and the discrete data from Hole 1262C confine the reversal to the interval between 115-116 mcd. The Hole 1262A data show a more gradual transition, but over an interval consistent with that seen in the other holes.

The new magnetostratigraphic interpretation is confirmed by the 20cm-spaced high-resolution calcareous nannofossil biostratigraphy we established for Site 1262. The NP10/NP11[4] (CP9a/CP9b[5]) boundary was observed at 118.5 ± 0.1 mcd, where the crossover in abundance between *Tribrachiatus contortus* and *T. orthostylus* is present. Other events which are related to the base of NP11 and maintain the same relative stratigraphic positions are from old to young: top of *Discoaster multiradiatus* at 119.6 ± 0.1 mcd, and the first occurrences of *Spenolithus radians* and *T. orthostylus* at 118.5 ± 0.1 mcd. This shows that NP10/NP11 (CP9a/CP9b) is positioned below the C24r/C24n reversal (and *Elmo* horizon), in accordance with the magnetobiostratigraphic results obtained from previous DSDP holes drilled at Walvis Ridge[6]. Furthermore, the lowermost occurrence of *T. orthostylus* was found at 295.75 ± 0.45 mcd in Site 1263, 282.25 ± 0.75 mcd in Site 1265, 295.89 ± 0.45 mcd in Site 1266, 208.35 ± 0.75 mcd in Site 1267, all confirming that the *Elmo* horizon is younger than the NP10/NP11 boundary.

Magnetic susceptibility and $CaCO_3$ weight% scales

The high-resolution MS/g records of Holes 1262A, 1263C, and 1266C were compared to the split core point magnetic susceptibility (PMS) and whole core MS of the multiple sensor track (MS-MST) measurements obtained during Leg 208[3]. We choose to convert all MS data to the MS-MST scale by performing linear regression analyses between MS/g and PMS (Supplementary Fig. 2a) and the conversion of PMS to MS-MST using the equation MST = PMS x 2.0683 + 7.8257 (R2 = 0.99)[3]. Subsequently, a regression analysis between the $CaCO_3$ weight% and the MS/g (converted to the MS-MST scale) of the same samples was applied (Supplementary Fig. 2b) to obtain the estimated $CaCO_3$ weight% scale of the various sites (Fig. 1).

Spectral results and astronomical tuning procedure

Power spectra were obtained by using the CLEAN transformation[7] and the Blackman-Tukey method[8]. For the determination of errors associated with the frequency spectra of the CLEAN algorithm, we applied a Monte Carlo based method[9]. Significance levels of 95, 97.5, 99 and 99.5% for the Monte Carlo spectra of the MS and L* depth series were determined by 1) 10% (i.e., Control parameter = 0.1) white noise addition, 2) Clean Gain factor of 0.1, 3) 500 CLEAN Iterations, 4) dt value of 0.02m, and 5) a total number of simulation iterations of 1000. The Blackman-Tukey power spectra were obtained by using the AnalySeries 1.1 software package[10]. In this case, data sets were equally spaced and prepared by removing the linear trends. Bandwidths of ~0.19 (Site 1262) and ~0.16 (Site 1267) have been applied as window to smooth the various spectra of the depth series.

The CLEAN[7,9] modulus and Blackman-Tukey[8,10] power spectra of L* and MS for Site 1262 revealed consistent and significant peaks at ~510, 123, 53, 38, 30 and 24.5cm (Supplementary Fig. 3). This frequency distribution of the spectral peaks is in good agreement with that of the astronomical cycles: the periodicities of these cycles equal 96 (short eccentricity), 41.5 (obliquity), 30 (obliquity), 23.5 (precession) and 19.5kyr (precession), respectively, if the ~510cm cycle is a reflection of the 405kyr[11] (long) eccentricity period. This assumption is consistent with the shipboard age model, which resulted in an average sedimentation rate for the early Eocene time interval at Site 1262 of ~1.2cm/kyr[3]. The correlative depth interval at Site 1267 revealed significant peaks in the L* spectra at ~570, and 146cm, and to a lesser degree at 58, and 32cm. The long and short eccentricity cycles thus appear to dominate the spectral distribution of this record, whereas the reflection of the obliquity and precession-related cycles is weak and diffuse.

To illustrate how we established the astronomical phase relationship for the extracted short and long eccentricity related MS and L* of Sites 1262 and 1267 (Fig. 3), a detail of the lithological changes in the interval just above the PETM of Site 1262 is shown in Supplementary Fig. 4. This interval clearly reflects the regular occurrence of pink coloured layers (p), which are repeatedly grouped in distinctive bundles of 2-3 layers. The 25-30cm spacing of successive pink coloured layers within one bundle corresponds to the precession-related spectral peaks (Supplementary Fig. 3), indicating that these layers are precession-forced. Evidently, the bundles are related to the short eccentricity-related MS maxima and are more frequently present during the long eccentricity-related MS maxima. In analogy to the well-known astronomical phase relations for the late

Neogene Mediterranean sapropel (=organic-enriched layer) record [12-14], the bundling of pink coloured layers should correspond to a maximum in eccentricity. Due to the eccentricity modulation of the climatic precession cycle, this orbital configuration should have lead to amplified seasonal contrasts on both Hemispheres and hence climate change, thereby triggering the deposition of the pink coloured layers, although it is yet not clear whether these layers should correspond to precession minima or maxima. The near absence of these layers during the long eccentricity-related MS minima further implies that these periods should correspond to minima in the ~405kyr eccentricity cycle, that weakens the effect of the ~100kyr modulation on climatic precession, and hence reduces the precessional-driven seasonal contrasts on both Hemispheres.

To investigate whether the very long orbital variations of ~2.25Myr have had an effect on the amplitude changes of the short eccentricity cycles between the PETM and *Elmo* horizon we extracted the ~100kyr component from the L* and MS records of Site 1262 by using a Gaussian filter centred at a frequency of 0.8125 ± 0.1 per meter (Supplementary Fig. 5). This analysis clearly revealed that the amplitude changes of the ~100kyr cycles are on-average less amplified during the second (II) ~405kyr related cycle of the L* and MS records from Site 1262 (Fig. 3). This spectral characteristic was compared with the minimum amplitude changes in the ~100kyr eccentricity cycles derived from R7[15] and La2004[11] orbital solutions using a Gaussian filter centred at a frequency of 0.0095 ± 0.002 per kyr (Supplementary Fig. 5). Subsequently, the extracted short and long eccentricity related components of the L* and MS records from Site 1262 were tuned using the most likely combination of both the ~2.25Myr related amplitude changes in the ~100kyr cycle and ~405kyr cycle (Fig. 3).

Global significance of the ETM2 event (and *Elmo* horizon)

To illustrate the global significance of the ETM2 event we compared our high-resolution $\delta^{13}C_{bulk}$ records across the *Elmo* horizon (this study) and PETM[16] of Site 1262 with those obtained from the subtropical Northwest Atlantic ODP Site 1051 and the high-latitude Southern Ocean ODP Site 690[17] (Supplementary Fig 6). These sites revealed a relatively strong negative excursion (termed H1) just below C24n/C24r (Site 1051) and within NP11 (Sites 690 and 1051), which bears strong resemblance with a similar negative excursion in the North Atlantic DSDP Site 550, and equatorial Pacific DSDP Site 577[17] (not shown). Given the good magnetobiostratigraphic constraints as well as the relative strength of this carbon isotope excursion with respect to that of the PETM, we conclude that the H1 is the equivalent of the ETM2 event. It should be noted that of all these sites only the magnetobiostratigraphy of Site 690 seems questionable, probably due to a series of unconformities immediately above the transient event H1 as indicated by the tight succession of the NP10/NP11, NP11/NP12, and NP12/NP14 zonal boundaries[18-20].

To further illustrate that the CIE associated with the ETM2 is not only recorded in the marine realm, we also plotted the paleosol soil nodule carbonate isotope record from the Bighorn Basin[21] in Supplementary Fig. 6. Although this record seems to reflect a noisy signal in some parts, the application of a 3 point moving average clearly demonstrate that the long-term Eocene $\delta^{13}C$ low is superimposed by two excursions: one definitely

related to the PETM and the other less amplified excursion in the interval just below the C24n/r boundary to, most likely, the ETM2 event.

References

1. Tauxe, L., Pick, T. & Kok, Y. S. Relative paleointensity in sediments: a pseudo-Thellier approach. *Geophysical Research Letters* **22**, 2885-2888 (1995).
2. Kirschvink, J. L. The least-squares line and plane and the analysis of paleomagnetic data. *Geophys. J. Roy. Astron. Soc.* **62**, 699-718 (1980).
3. Zachos, J. C., Kroon, D., Blum, P. & al., e. *Early Cenozoic Extreme Climates: The Walvis Ridge Transect* (eds. Zachos, J. C., Kroon, D. & Blum, P.) (2004).
4. Martini, E. in *Planktonic Conference* (ed. Farinacci, A.) 739-785 (Tecnosci, Roma, 1971).
5. Okada, H. & Bukry, D. Supplementary modification and introduction of code numbers to the low-latitude coccolith biostratigraphic zonation (Bukry, 1973; 1975). *Mar. Micropaleontol.* **5**, 321-325 (1980).
6. Backman, J. Late Paleocene to middle Eocene calcareous nannofossil biochronology from Shatsky Rise, Walvis Ridge and Italy. *Palaeo Geography Climatology Ecology* **57**, 43-59 (1986).
7. Roberts, D. H., Lehar, J. & Dreher, J. W. Time series analysis with CLEAN. Part I. Derivation of a spectrum. *Astron. J.* **93**, 968-989 (1987).
8. Blackman, R. B. & Tukey, J. W. *The Measurement of Power Spectra From the Point of View of Communication Engineering.* (Dover Publications, New York, 1958).
9. Heslop, D. & Dekkers, M. J. Spectral analysis of unevenly spaced climatic time series using CLEAN: signal recovery and derivation of significance levels using a Monte Carlo simulation. *Physics of the Earth and Planetary Interiors* **130**, 103-116 (2002).
10. Paillard, D., Labeyrie, L. & Yiou, P. Macintosh Program Performs Time-Series Analysis. *Eos Trans. AGU* **77**, 379 (1996).
11. Laskar, J. et al. A long term numerical solution for the insolation quantities of Earth. *Astronomy and Astrophysics* **428**, 261-285 (2004).
12. Hilgen, F. J. Astronomical calibration of Gauss to Matuyama sapropels in the Mediterranean and implication for the geomagnetic polarity time scale. *Earth Planet. Sci. Lett.* **104**, 226-244 (1991).
13. Lourens, L. J. et al. Evaluation of the Plio-Pleistocene astronomical timescale. *Paleoceanography* **11**, 391-413 (1996).
14. Hilgen, F. J. et al. Extending the astronomical (polarity) time scale into the Miocene. *Earth Planet. Sci. Lett.* **136**, 495-510 (1995).
15. Varadi, F., Bunnegar, B. & Ghil, M. Successive refinements in long-term integrations of planetary orbits. *Astrophysical J.* **592**, 620-630 (2003).
16. Zachos, J. C. et al. Rapid Acidification of the Ocean during the Paleocene-Eocene Thermal Maximum. *Science* (in press).
17. Cramer, B. S., Wright, J. D., Kent, D. V. & Aubry, M.-P. Orbital climate forcing of d13C excursions in the late Paleocene–early Eocene (chrons C24n–C25n). *Paleoceanography* **18**, 10.1029/2003PA000909 (2003).

18. Berggren, W. A. & Aubry, M.-P. in *Correlation of the Early Paleogene in Northwset Europe, Special Publication* (eds. Knox, R. W. O. B., Corfield, R. M. & Dunay, R. E.) (Geol. Soc., London, 1996).
19. Aubry, M.-P., Berggren, W. A., Stott, L. D. & Sinha, A. in *Correlation of the Early Paleogene in Northwest Europe, Special Publication* (eds. Knox, R. W. O. B., Corfield, R. M. & Dunay, R. E.) (Geol. Soc., London, 1996).
20. Ali, J., Kent, D. V. & Hailwood, E. Magnetostratigraphic reinvestigation of the Palaeocene/Eocene boundary interval in Hole 690B, Maud Rise. *Geoph. J. Int.* **141**, 639-646 (2000).
21. Koch, P. L. et al. in *Causes and Consequences of Globally Warm Climates in the Early Paleogene* (eds. Wing, S. L., Gingerich, P. D., Schmitz, B. & Thomas, E.) 49-64 (Geological Society of America Special Paper, Boulder, Colorado, 2003).

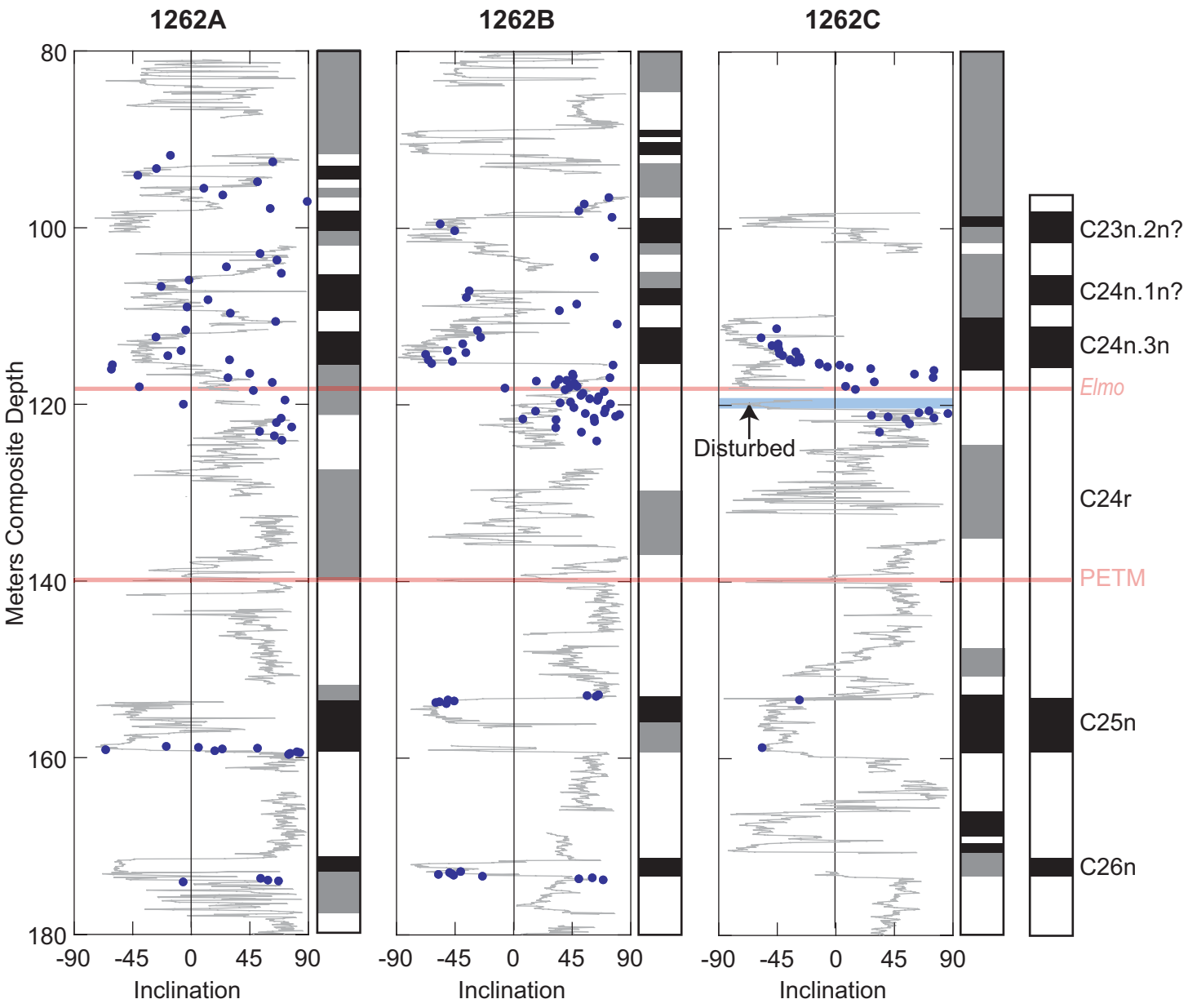

Supplementary Figure 1 Late Palaeocene to early Eocene magnetostratigraphy for ODP Site 1262. Shipboard pass-through inclination (demagnetized to 15 mT; grey lines) and discrete sample inclination (principle component calculated from 20 to 40 mT; blue circles). Shaded interval on site 1262C represents a particularly disturbed core section, results from which should not be considered reliable. Overall magnetostratigraphic interpretation to right. Black = normal polarity; white = reverse; grey = indeterminate.

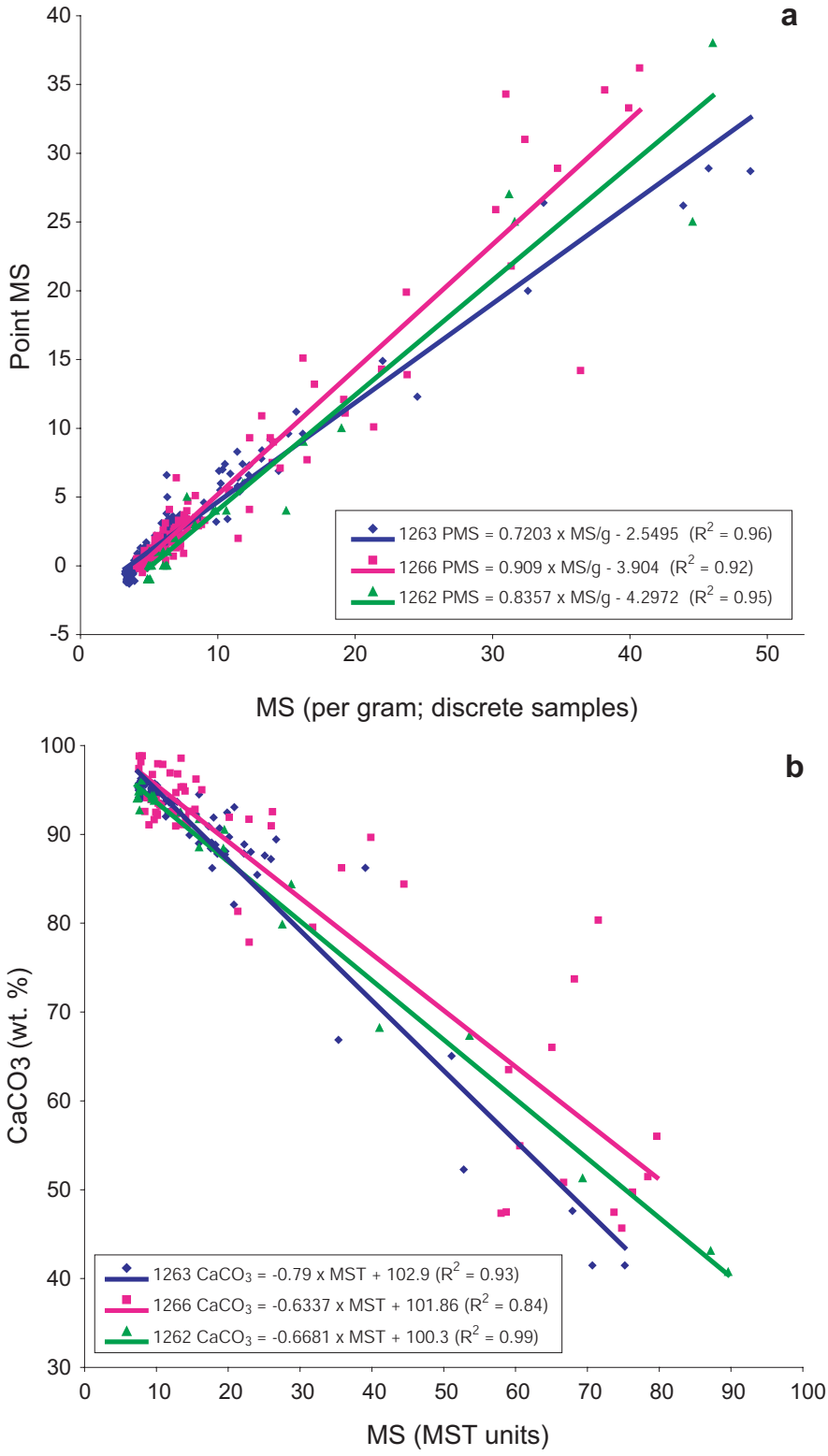

Supplementary Figure 2 Regression analyses for the magnetic susceptibility to calcium carbonate weight percentage conversion of Sites 1262, 1263 and 1267. **a**, Magnetic susceptibility per gram sediment (MS/g) versus shipboard point magnetic susceptibility (PMS). The MS/g values were converted to the shipboard magnetic susceptibility scale of the multi sensor track (MS-MST) using the displayed function for each site and the equation MS-MST = PMS x 2.0683 + 7.8257 (R2 = 0.99) (Ref. 3). **b**, MS/g (on the recalibrated MS-MST scale) versus CaCO3 weight%.

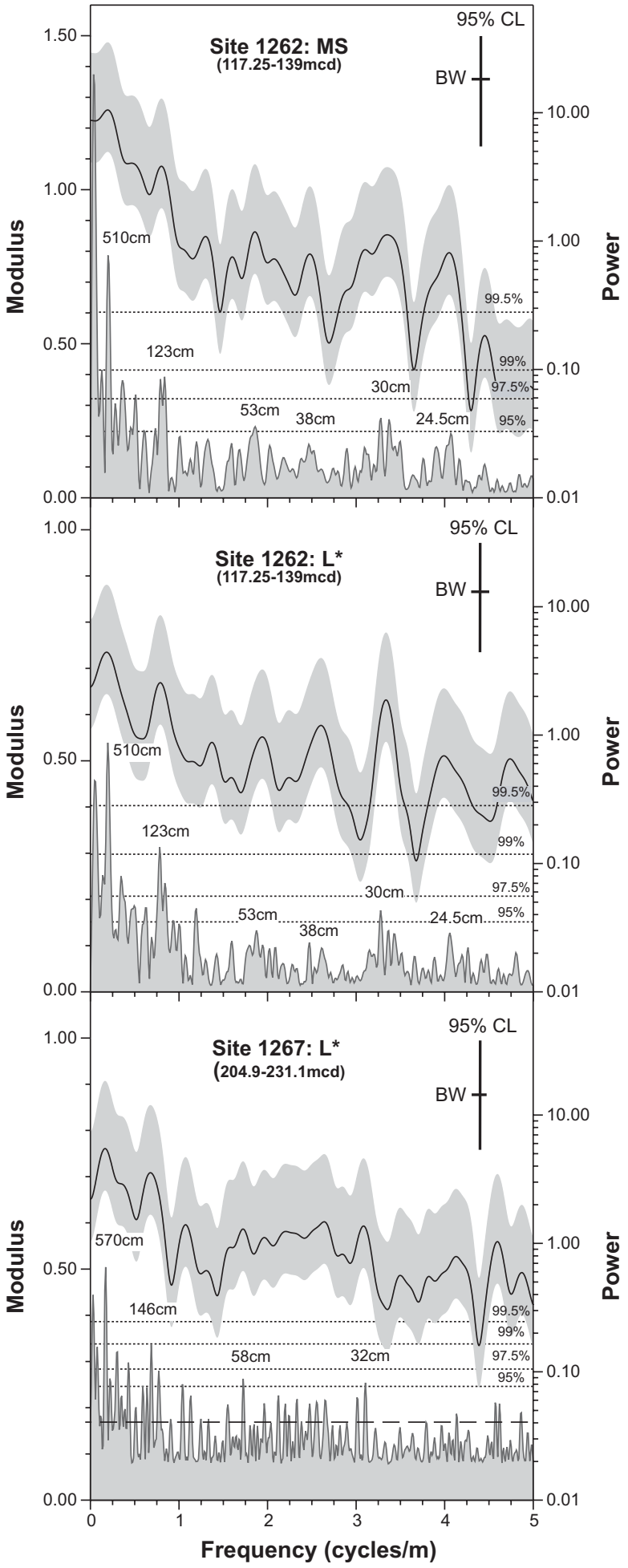

Supplementary Figure 3 Frequency spectra of the magnetic susceptibility and color reflectance records of Sites 1262 and 1267 for the *Elmo*-PETM interval. Results of the CLEAN-algorithm and Blackman-Tukey (BT) are expressed by their modulus and power, respectively. Horizontal dotted lines indicate the 95, 97.5, 99, and 99.5% significance level of the CLEANED-spectra. Bandwidth (BW) and 95% confidence limits (CF) of the BT spectra are based on a Tukey window with a number of lags that equal 30% the length of the data series.

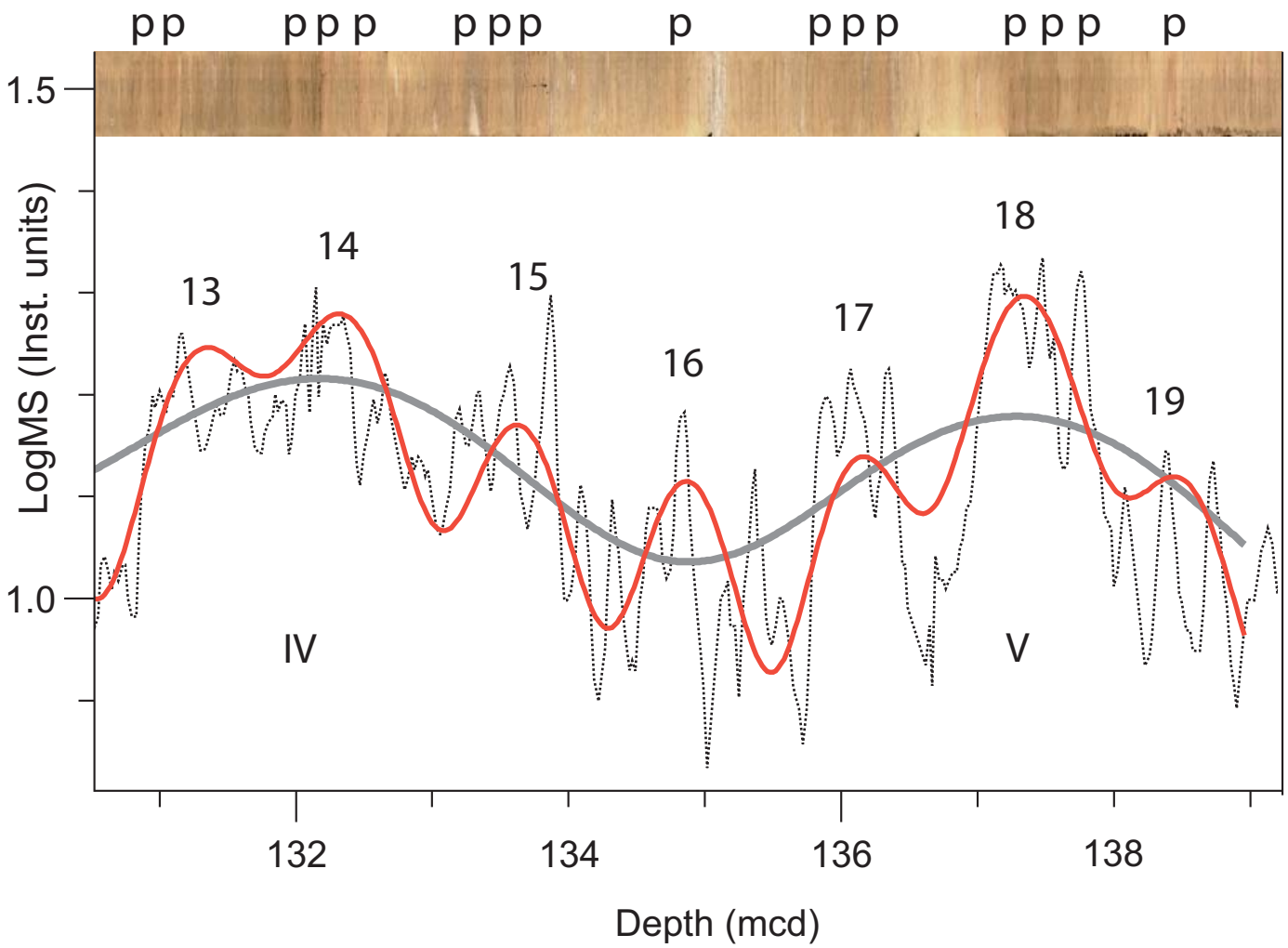

Supplementary Figure 4 Comparison between precession-related lithological changes and eccentricity cycles in the magnetic susceptibility record of Site 1262. The pink-coloured layers, related to precession, are particularly distinctive during maxima in the short and long-term eccentricity related cycles of the MS record.

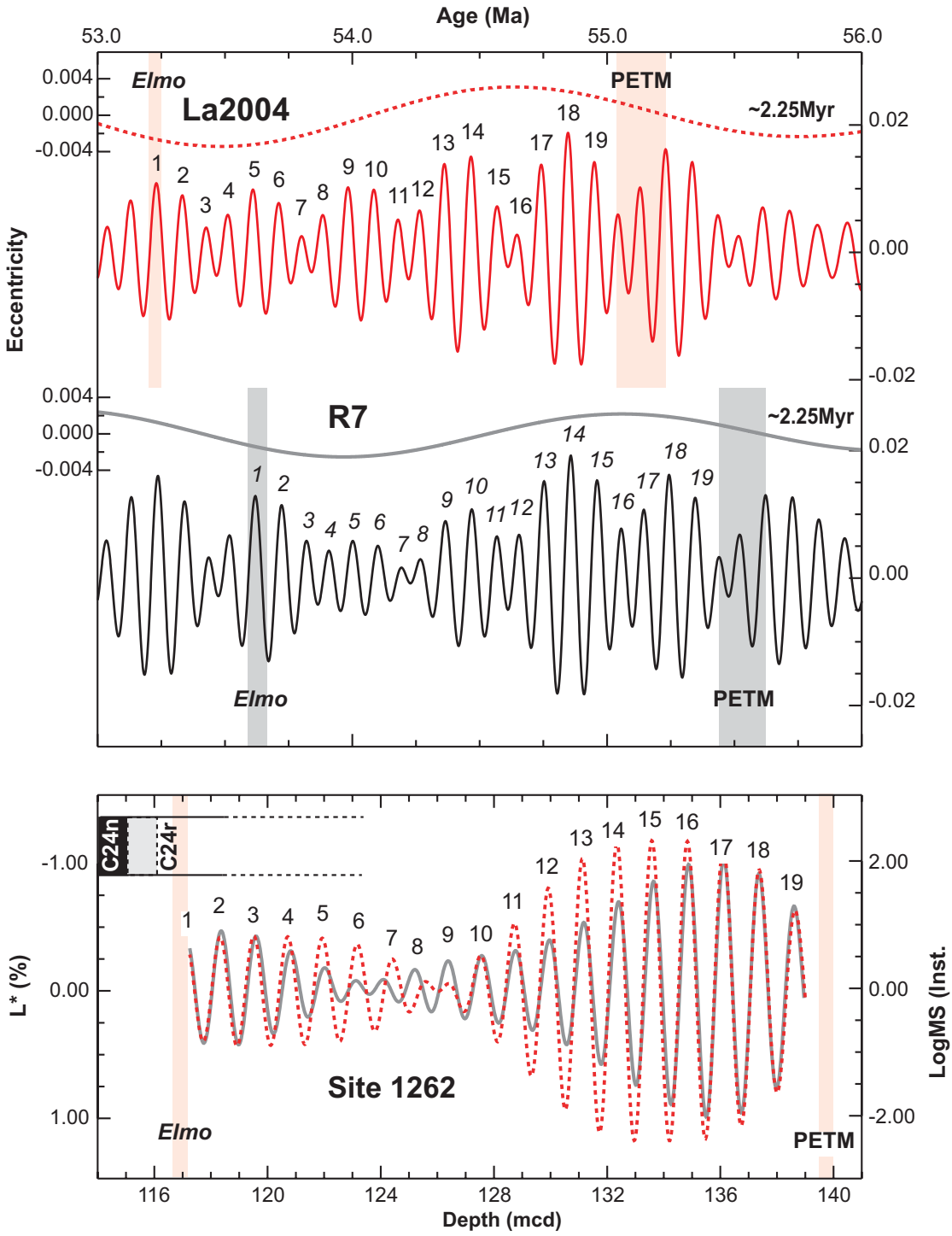

Supplementary Figure 5 Amplitude modulation of the ~100kyr eccentricity components in Site 1262 and orbital computations. Gaussian filters centred at a frequency of 0.0095 ± 0.002 per kyr and 0.8125 ± 0.1 per meter were applied to extract the ~100kyr eccentricity components from the R7 (Ref. 15) and La2004 (Ref. 11) orbital solutions and their correlative cycles from the L* (solid) and MS (dot) records of Site 1262, respectively.

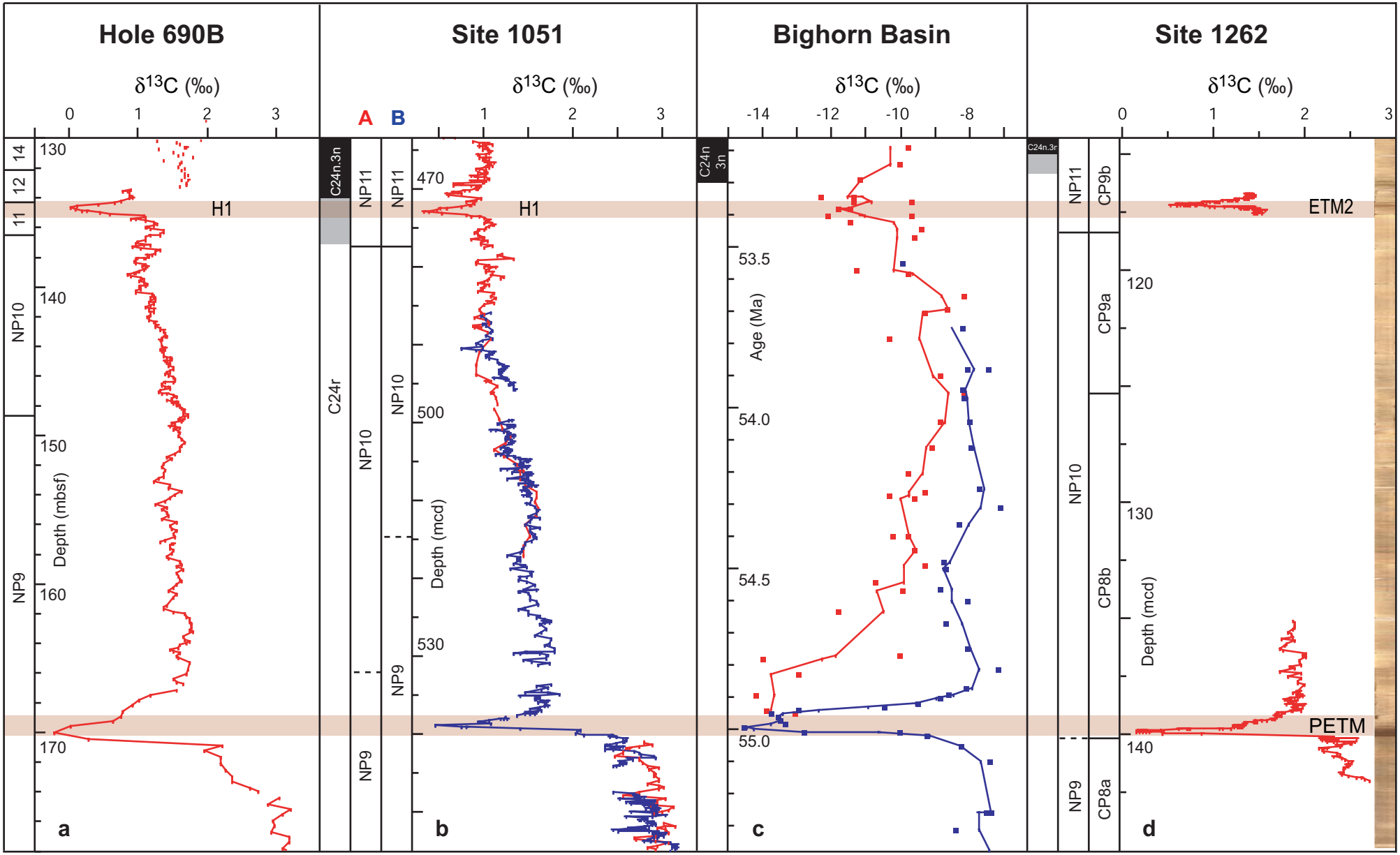

Supplementary Figure 6 Global registration of the PETM and *Elmo* carbon isotope excursions in four well-dated (magneto- and/or nannofossil stratigraphy) sections. **a**, ODP Hole 690B (Southern Ocean) (Ref. 17). **b**, ODP Holes 1051A (red) and 1051B (blue) (Blake Nose, Northwestern Atlantic) (Ref. 17). **c**, Paleosol carbonate isotope record from the Bighorn Basin (Wyoming, USA) (Ref. 21). **d**, ODP Site 1262 (this study) and PETM (Ref. 16).